Scaling Properties in the Production Range of Shear Dominated Flows

C. M. Casciola, P. Gualtieri, B. Jacob, and R. Piva

Dipartimento di Meccanica e Aeronautica, Università di Roma La Sapienza, Via Eudossiana 18, 00184 Roma, Italy

(Received 11 January 2005; published 7 July 2005)

In large Reynolds number turbulence, isotropy is recovered as the scale is reduced and homogeneous-isotropic scalings are eventually observed. This picture is violated in many cases, e.g., wall bounded flows, where, due to the shear, different scaling laws emerge. This effect has been ascribed to the contamination of the inertial range by the larger anisotropic scales. The issue is addressed here by analyzing both numerical and experimental data for a homogeneous shear flow. In fact, under strong shear, the alteration of the scaling exponents is not induced by the contamination from the anisotropic sectors. Actually, the exponents are universal properties of the isotropic component of the structure functions of shear dominated flows. The implications are discussed in the context of turbulence near solid walls, where improved closure models would be advisable.

DOI: 10.1103/PhysRevLett.95.024503 PACS numbers: 47.27.Nz

Introduction.—One of the issues in fluid dynamics concerns the small scale behavior of turbulence. According to Kolmogorov, turbulent flows at sufficiently large Reynolds number develop a range of scales, much smaller than the integral scale of the system, where the dynamics is isotropic, universal, and independent of viscosity. Statistical observables, such as moments of velocity increments, are then expected to exhibit power laws in terms of separation with universal exponents. These scaling laws are normally exploited in closures for the Navier-Stokes equations, coarse grained at inertial scales. However, inertial range predictions are often violated and this entails the failure of the related closures, like it happens in shear dominated flows, e.g., boundary layers near solid walls.

Actually, shear flows exhibit distinct ranges of scales, see Fig. 1 for nomenclature and definitions. When the Reynolds number is sufficiently large, a classical inertial subrange [1] sets in between the dissipative scale, η, and the energy injection scale, l. In equilibrium shear flows, where production and dissipation balance, $l = L_s = \sqrt{\epsilon/S^3}$. In the inertial subrange the longitudinal spectrum behaves like $E_{xx}(k_x) \propto \epsilon^{2/3} k_x^{-5/3}$, and the longitudinal structure functions exhibit scaling laws, $S_n \propto r_x^{\zeta(n)}$ [2], with exponents consistent with homogeneous-isotropic data. There is however a residual effect of the anisotropy, as shown by the nth order structure tensors $S^{(n)}_{\alpha_1,\ldots,\alpha_n}(r_\beta) = \langle \delta u_{\alpha_1} \ldots \delta u_{\alpha_n} \rangle$, where $\delta u_\alpha = u_\alpha(x_\beta + r_\beta) - u_\alpha(x_\beta)$ [3]. The proper tool to address this issue is by projecting the relevant tensors on the invariant subspaces of the rotation group, the so-called SO(3) decomposition. Because of the rotational invariance of the Navier-Stokes equations, such SO(3) components are found to manifest pure scaling laws in terms of separation $r = \sqrt{r_\alpha r_\alpha}$. The exponents are independent of the flow details and the isotropic sector behaves exactly as in isotropic turbulence. In the inertial subrange, the anisotropic contributions are subleading and the isotropic sector controls the small scale asymptotics [3–5]. All these results rest on the assumption that, at inertial scales, anisotropy is at most a weak perturbation of an otherwise isotropic dynamics.

The production range of shear flows is less understood. There, a perturbation approach cannot work, since anisotropy is the prominent characteristic. Also, in the production range, however, certain features seem to be universal. Relative exponents—$\zeta_{rel}(n) = \zeta(n)/\zeta(3)$ [6]—show systematic differences with respect to classical results [7–9] and consistent deviations are found in direct numerical

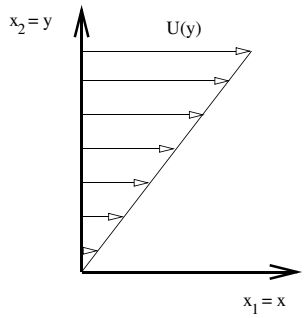

FIG. 1. Sketch of the shear flow and nomenclature: the mean flow $U(y)$, in the $x \equiv x_1$ direction, is a function of $y \equiv x_2$, with $z \equiv x_3$. For a linear mean profile, the shear rate $S = dU/dy$ is constant and the flow is spatially homogeneous. In wall bounded flows the shear rate depends on distance from the wall. The field is the sum of average and fluctuation, with the latter denoted by u_α, $\alpha = 1, 2, 3$—i.e., $u_{x/y/z}$, or u, v, w. The production of turbulent kinetic energy is $\Pi = S\langle u_x u_y \rangle$, where $\langle u_x u_y \rangle$ is the relevant component of the Reynolds tensor $\langle u_\alpha u_\beta \rangle$. The square root of its trace is the fluctuation intensity $q_{rms} = \sqrt{\langle u_\alpha u_\alpha \rangle}$. The dissipation rate is $\epsilon = \langle 1/2\nu(\partial u_\alpha/\partial x_\beta + \partial u_\beta/\partial x_\alpha) \times (\partial u_\alpha/\partial x_\beta + \partial u_\beta/\partial x_\alpha) \rangle$, where ν is the kinematic viscosity of the fluid. The Kolmogorov dissipative scale is given by $\eta = (\nu^3/\epsilon)^{1/4}$ and the Taylor microscale is defined via $\epsilon = 5\nu q_{rms}^2/\lambda^2$. $Re_\lambda = \lambda q_{rms}/\nu$ is the relevant form of the Reynolds number.

simulations (DNS), either in the presence [10–12] or absence of solid boundaries [13]. All these indications support the conjecture of a universal regime. Actually, in [11], by analyzing DNS results for a channel flow through the so-called extended self-similarity approach [6], a new form of scaling law was devised for longitudinal structure functions in the production range, as confirmed by experimental data from a boundary layer [8]. In [12], using experimental data, a combined form of longitudinal structure function was proposed, able to incorporate both scaling laws for the inertial and the production range in a single composite observable with the same scaling exponents of standard homogeneous-isotropic turbulence; see also [13] for related aspects. However, the origin of these scalings has never been addressed so far. Actually, the asymptotic approach for small shear may lead one to believe that, in the standard longitudinal structure functions, the isotropic scalings would disappear due to contamination from the anisotropic sectors that would spoil the classical power laws at large scales. In fact, we find here that the origin of the observed alteration in the longitudinal structure functions is by no way induced by contamination. It is instead the behavior of the isotropic sector itself to be dramatically modified by the shear.

Several reasons may have prevented the identification of the physical origin of the shear dominated scaling regime, $S_n(r) \propto r^{\zeta_S(n)}$. On the one hand, limitations on the Reynolds number of present-day DNS hinder the direct observation of scaling laws. On the other hand, experiments cannot provide the spatial information to distinguish the contributions of different SO(3) sectors and this, as we shall see, may lead to an ambiguous physical interpretation.

The purpose of the present Letter is to address shear dominated scaling laws in the simplest conditions of a homogeneous shear flow, see Fig. 1. The combined use of experimental and numerical data will enable us to extract the exponents for the isotropic sector to a sufficient degree of accuracy to claim that their values definitely differ from those of the inertial subrange.

We address different data sets. The experimental ones are described in [14]. The others are provided by highly resolved large eddy simulations (LES) at three different shear intensities. The LES approach by achieving sufficiently large Reynolds numbers allows for scaling laws in terms of separation to emerge in a much neater way that would otherwise be possible by DNS.

Large eddy simulation.—In LES the coarse grained field $\bar{u}_\alpha(x_\beta, t)$ is related to the fine grained field $u_\alpha(x_\beta, t)$ via a spatial filter $\mathcal{G}$ with cutoff length Δ (see details in note [15] at the end of the Letter and the reference there provided),

$$\bar{u}_\alpha(x_\beta, t) = \int G_\Delta(x_\beta - \tilde{x}_\beta) u_\alpha(\tilde{x}_\beta, t) d^3\tilde{x}. \qquad (1)$$

The flow has the mean profile sketched in Fig. 1 and periodic initial conditions on the fluctuating field. The equation for the coarse grained solenoidal field is

$$\frac{\partial \bar{u}_\alpha}{\partial t} = \epsilon_{\alpha\beta\gamma}\overline{u_\beta \zeta_\gamma} - \partial_\alpha \bar{\pi} + \nu \partial_{\beta\beta}\bar{u}_\alpha - S\bar{u}_y\delta_{\alpha 1} - \frac{\partial \overline{u_\alpha U}}{\partial x}, \qquad (2)$$

where π is the sum of pressure and kinetic energy density and the permutation symbol $\epsilon_{\alpha\beta\gamma}$ performs the cross product between velocity and its curl ζ_α.

Equation (2) alone is insufficient to determine $\bar{u}_\alpha$ and a suitable closure is needed. The approximate deconvolution method (additional information on the ADM is given in note [16]; see also the related reference) uses an approximate inversion of the filter to reconstruct u_α from $\bar{u}_\alpha$ and evaluate the unclosed terms $\epsilon_{\alpha\beta\gamma}\overline{u_\beta\zeta_\gamma}$ and $\overline{u_\alpha U}$.

The LES simulation follows the standard, state-of-the-art numerical procedure devised for the DNS of homogeneous turbulence subject to uniform shear [17,18], which makes use of the remeshing procedure proposed by Rogallo. In this kind of simulation the global turbulent kinetic energy is found to manifest large intermittency cycles. They are not an artifact of the numerical procedure, as confirmed by their time scales, which are typically 1 order of magnitude larger than the remeshing period.

We emphasize that our LES is actually very close to a DNS, since the filter cutoff Δ is always much smaller than L_s to have the solution virtually unaffected by the model in

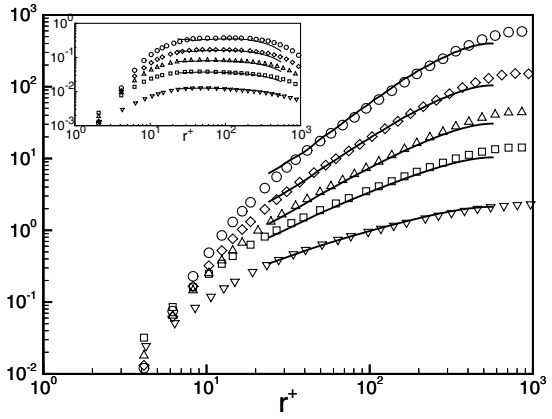

FIG. 2. Longitudinal structure functions vs separation, experiments (symbols)—$n = 2$ (triangles), $n = 3$ (squares), $n = 4$ (delta), $n = 5$ (diamonds), and $n = 6$ (circles)—and LES (solid line). Moments $n = 3, 4, 5, 6$ are multiplied by 2. Data normalized by $q_{\rm rms}$, $r^+ = r/\eta$. In the experiment $\Pi \simeq \epsilon \simeq 0.85\ {\rm m^2\,s^{-3}}$, $S \simeq 19\ {\rm s^{-1}}$, $q_{\rm rms} \simeq \sqrt{u_{\rm rms}^2 + 2v_{\rm rms}^2} \simeq 0.6\ {\rm ms^{-1}}$, $S^* \simeq 8$, and ${\rm Re}_\lambda \simeq 220$. LES at $S^* = 7$ and ${\rm Re}_\lambda = 150$, $\Delta^+ = \Delta/\eta = 17$, $L_s^+ = L_s/\eta = 70$. Computational box: $L_x = 4\pi$, $L_y = 2\pi$, $L_z = 2\pi$, with $L_x^+ = 1250$. Concerning the integral scale $L = q_{\rm rms}^3/\epsilon$, $L^+ = L/\eta = 1400$. In the inset, the same data in compensated form, $S_n/r^{\zeta_s(n)}$, same symbols: $\zeta_s(n) = 0.72, 1.00, 1.23, 1.42, 1.58$, for $n = 2, 3, 4, 5, 6$, respectively, (For isotropic flows $\zeta(n) = 0.69, 1.00, 1.28, 1.54, 1.78$).

the production range (precise data are provided in the figure captions). The resolution is $N_x \times N_y \times N_z = 192 \times 216 \times 96$, with $St_{\max} \simeq 500$ and $Dt(\epsilon/\eta^2)^{1/3} \simeq .03$.

Scalings in the shear dominated range.—The homogeneous shear flow is characterized by two independent parameters, $S^* = Sq_{\rm rms}^2/\epsilon$ and $\mathrm{Re}_\lambda = q_{\rm rms}\lambda/\nu$. Longitudinal structure functions

$$S_n(r_x) = \langle [u_x(x + r_x, y, z) - u_x(x, y, z)]^n \rangle \qquad (3)$$

from simulations and experiments are compared in Fig. 2. The simulation was designed to reproduce the conditions of the experiments, as shown in the figure, where in the two cases—experiments and LES—the structure functions agree very well. A scaling behavior in terms of separation is clearly inferred from the plots and confirmed by the inset. Experiments and numerics provide identical exponents. In comparison, the exponents of isotropic turbulence are considerably different, see figure caption.

Longitudinal structure functions follow from the superposition of all the SO(3) sectors [3],

$$S_n(r_x) = \sum_{j=0}^{\infty} \sum_{m=-j}^{j} S_{jm}^{(n)}(r) Y_{jm}(0, 0), \qquad (4)$$

where $Y_{jm}(\theta, \phi)$ are the spherical harmonics in terms of polar, θ, and azimuthal, ϕ, angles. Here j denotes the sector, with $j = 0$ the isotropic contribution independent of the orientation of the radial vector, and $S_{jm}^{(n)}(r)$ the components of the structure function in the jth sector. Because of the strict homogeneity of the flow, the spherical harmonics provide the natural basis to address the angular dependence of the structure functions also in the range of large separations. The same tool could be inappropriate to deal with the large scales of inhomogeneous flows, such as boundary layers or channel flows.

In principle, scaling laws in the different sectors with j-dependent exponents, $S_{jm}^{(n)}(r) \propto r^{\zeta_j(n)}$, may lead to a blending of power laws, and to an effective logarithmic slope in the complete longitudinal structure functions. If this is the case, the effective slope would strongly depend on the relative intensity of the different sectors, resulting in a highly flow dependent feature. We will see below that the scaling laws emerge in a different way.

In order to ascertain the physical origin of the scalings reported in Fig. 2 it is appropriate to extract the dominant contributions from the general SO(3) decomposition. The interest is naturally focused on the isotropic sector, $j = 0$. Unfortunately, experimental data can hardly be used to cleanly extract the pure isotropic component, $S_{00}^{(n)}(r)$, due to the lack of spatial information. However, this is easily done on the basis of numerical data, considering that $Y_{00}(\theta, \phi) \equiv 1/\sqrt{4\pi}$, so that

$$S_{00}^{(n)}(r) = \frac{1}{\sqrt{4\pi}} \int_0^{\pi} \int_0^{2\pi} S_n(r_x, r_y, r_z) \sin(\theta) d\theta d\phi. \qquad (5)$$

Results for $n = 6$, where the difference between the exponent of the longitudinal structure function—$\zeta_s(6) = 1.58$—and that of isotropic turbulence—$\zeta(6) = 1.78$—is particularly large, are reported in Fig. 3. Here the isotropic contribution $S_{00}^{(6)}(r)$ is plotted for three different shear intensities S^*. The first one, the high shear case (circles), is the same we have already discussed. It is clear from the plot that 1.58 (solid line) is the appropriate exponent to achieve compensation. It is also clear from the figure that the classical isotropic value of 1.78 (dashed lines) is unsuitable to fit the data. We conclude that a pure scaling law with an exponent considerably smaller than the isotropic one characterizes the isotropic sector of this shear dominated flow. This exponent is able to fit also the longitudinal structure functions, as already shown in Fig. 2. The SO(3) decomposition allows here to exclude contamination effects from the anisotropic sectors.

The difference between 1.58 and 1.78 represents the shear-induced alteration of the exponent in the isotropic sector of the sixth order structure function. Contrary to expectation, this effect is not a flow dependent superposition of universal exponents of all sectors, but the modification of the exponent of the isotropic sector itself.

As we may expect from the previous analysis, below the shear scale we recover the isotropic exponents. Going below L_s while still remaining sufficiently apart from dissipative effects requires some care in the homogeneous shear flow. To this purpose we have selected the low shear case defined in Fig. 3 (triangles) [19,20]. The plots in the figure are self-explanatory: below the shear scale we ac-

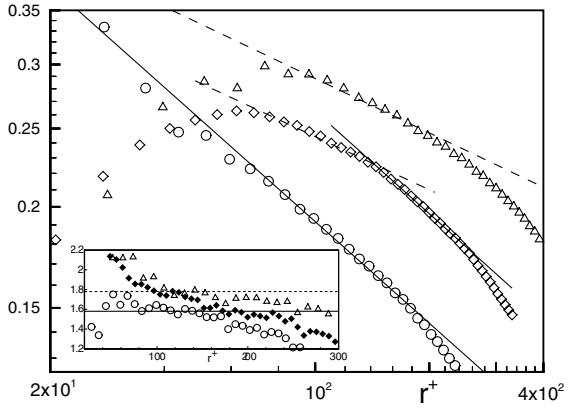

FIG. 3. Isotropic component of the sixth order longitudinal structure function normalized by its dimensional scaling, $S_{00}^{(6)}/r^2$. High shear case: circles, parameters defined in the caption of Fig. 2. Low shear case: triangles, $S^* = 2.2$, $\mathrm{Re}_\lambda = 160$, $L_s^+ = 430$, $L^+ = 1325$, $L_x^+ = 1630$, $\Delta^+ = \Delta/\eta = 20$. Intermediate shear case: diamonds, $S^* = 5.4$, $\mathrm{Re}_\lambda = 150$, $L_s^+ = 110$, $L^+ = 1320$, $L_x^+ = 1320$, $\Delta^+ = \Delta/\eta = 17$. The slope of the solid lines is -0.42, corresponding to $\zeta_s(6) = 1.58 \pm 0.08$. For the dashed lines the slope is -0.22, i.e., $\zeta(6) = 1.78 \pm 0.08$. In the inset, the local slope (diamonds filled for better readability).

tually reproduce the results of isotropic turbulence. Ideally, when the shear scale lays in the middle of the scaling range, one should observe the simultaneous presence of the two scaling behaviors. This is what happens indeed in the third case (diamonds) where the isotropic component of the sixth order structure function scales with $\zeta(6) = 1.78$ (dashed line) at small scales and with $\zeta_s(6) = 1.58$ at large scales. With acceptable precision, the crossover is found at $r = L_s$.

Final comments.—In conclusion, we have addressed the scaling laws for the isotropic component of structure functions in the shear dominated range of the homogeneous shear flow. The exponents are lower than those of the classical inertial subrange, in agreement with previous results for longitudinal structure functions in the production range. The aim was to understand the origin of such alteration. Were it due to contamination from the anisotropic sectors, scaling laws would result as intensity-dependent superpositions of the exponents of each sector. The issuing effective exponent would be a strongly flow dependent feature. We show instead that longitudinal structure functions change under shear essentially as a consequence of the shear-induced alteration of the isotropic sector. This gives reason to the experimental observations that, in the appropriate range of scales, always the same values of the exponents are reproduced. Actually, all the data available to us—channel flows, boundary layers at different distance from the wall, homogeneous shear flows, and presumably even jets—yield the same exponents we have produced here. In other words, the production range of shear flows seems to be characterized by the universal set of scaling exponents inherited by the isotropic sector and provided in Fig. 2. In applications such universality is instrumental for developing proper closures for LES, which are actually needed since those based on classical Kolmogorov-like arguments are known to fail close to the wall.

[1] A. N. Kolmogorov, Dokl. Akad. Nauk SSSR **30**, 299 (1941).

[2] A. Arneodo *et al.*, Europhys. Lett. **34**, 411 (1996).

[3] I. Arad, V. S. L'vov, and I. Procaccia, Phys. Rev. E **59**, 6753 (1999). Longitudinal structure functions are obtained from the correlation tensor by contraction with the unit radial vector, $S_n(r_x, r_y, r_z) = S^{(n)}_{\alpha_1,\ldots,\alpha_n}(r_\beta)\hat{r}_{\alpha_1}\ldots\hat{r}_{\alpha_n} - S_n(r_x) = S_n(r_x, 0, 0)$. As scalars, they are expanded in terms of spherical harmonics. For the general SO(3) decomposition of tensorial objects see the referenced paper; L. Biferale and I. Procaccia, Phys. Rep. **414**, 43 (2005).

[4] I. Arad, B. Dhruva, S. Kurien, V. S. L'vov, I. Procaccia, and K. R. Sreenivasan, Phys. Rev. Lett. **81**, 5330 (1998).

[5] L. Biferale and F. Toschi, Phys. Rev. Lett. **86**, 4831 (2001).

[6] R. Benzi, S. Ciliberto, C. Baudet, and G. Ruiz-Chavarria, Physica D (Amsterdam) **80**, 385 (1995). When $S_3 \propto r$, scaling laws can be rearranged in extended self-similarity form $S_n \propto S_3^{\xi(n)}$. This form of similarity has a much wider range of application than the original one in physical separation. More generally, assuming $S_3 \propto r^{\zeta(3)}$, $S_n \propto S_3^{\xi_{\rm rel}(n)}$.

[7] G. Ruiz-Chavarria, S. Ciliberto, C. Baudet, and E. Lévêque, Physica D (Amsterdam) **141**, 183 (2000).

[8] B. Jacob, A. Olivieri, and C. Casciola, Phys. Fluids **14**, 481 (2002).

[9] C. M. Casciola, R. Benzi, P. Gualtieri, B. Jacob, and R. Piva, Phys. Rev. E **65**, 015301(R) (2002).

[10] F. Toschi, G. Amati, S. Succi, R. Benzi, and R. Piva, Phys. Rev. Lett. **82**, 5044 (1999).

[11] R. Benzi, G. Amati, C. M. Casciola, F. Toschi, and R. Piva, Phys. Fluids **11**, 1 (1999).

[12] F. Toschi, E. Lévêque, and G. Ruiz-Chavarria, Phys. Rev. Lett. **85**, 1436 (2000).

[13] C. M. Casciola, P. Gualtieri, R. Benzi, and R. Piva, J. Fluid Mech. **476**, 105 (2003).

[14] B. Jacob, L. Biferale, G. Iuso, and C. M. Casciola, Phys. Fluids **16**, 4135 (2004). A stream is forced through a system of channels each with a different head loss. They discharge in a uniform ambient pressure and produce a nominally linear velocity profile sufficiently downstream. There, hot wires acquire the streamwise velocity and give access to the longitudinal structure functions.

[15] O. V. Vasilyev, T. S. Lund, and P. Moin, J. Comput. Phys. **146**, 82 (1998). The kernel G_Δ is invariant under translations, vanishes rapidly, and filtering commutes with differentiation. It is expressed as the Cartesian product of one-dimensional filters $g_\Delta(x) = 1/\Delta g_1(x/\Delta)$, controlled by the moments $M_n = \int \xi^n g_1(\xi) d\xi$. Here $M_n = 0$ for $n = 1, \ldots, 5$ with additional conditions on the Fourier transform $\hat{g}_1(0) = \hat{g}_1(\pi) = 0$, $d\hat{g}_1(\pi)/d\omega = 0$, where ω is the wave number normalized by Δ. The roll-off is such that $\hat{g}_1(3\pi/4) = 1/2$.

[16] S. Stolz and A. Adams, Phys. Fluids **11**, 1699 (1999), the approximate inverse is given by $\mathcal{Q}_N = \Sigma_{n=1}^N (\mathcal{I} - \mathcal{G})^n \simeq \mathcal{G}^{-1}$, with $N = 5$. To stabilize the scales below the cutoff, the additional term $\sigma_\alpha = -\chi_u(\mathcal{I} - \mathcal{Q}_N\mathcal{G})\bar{u}_\alpha$, with $\chi_u = 40S$, is also introduced in Eq. (2).

[17] A. Pumir and B. I. Shraiman, Phys. Rev. Lett. **75**, 3114 (1995).

[18] P. Gualtieri, C. M. Casciola, R. Benzi, G. Amati, and R. Piva, Phys. Fluids **14**, 583 (2002).In the variables $X_1 = x_1 - U(x_2)t$, $X_2 = x_2$, $X_3 = x_3$ the fluctuations are periodic and spectral methods can be used, as proposed by Rogallo. The configuration is cyclically mapped back to the original box after a period of $L_x/(SL_y)$.

[19] X. Shen and Z. Warhaft, Phys. Fluids **12**, 2976 (2000), the two parameters of the flow, S^* and Re_λ, cannot be varied independently, unless active grids are introduced to stir the fluid.

[20] J. Schumacher, Phys. Fluids **16**, 3094 (2004). In numerical simulations a random forcing at large scales is used to achieve the substantial enhancement of the shear scale needed here.